ACS OMEGA

http://pubs.acs.org/journal/acsodf

Article

Spatiotemporal Patterning Enabled by Gene Regulatory Networks

Ushasi Roy,*[,¶] Divyoj Singh,[¶] Navin Vincent,[§] Chinmay K. Haritas,[§] and Mohit Kumar Jolly*

Cite This: *ACS Omega* 2023, 8, 3713−3725

Read Online

ACCESS | Metrics & More | Article Recommendations | Supporting Information

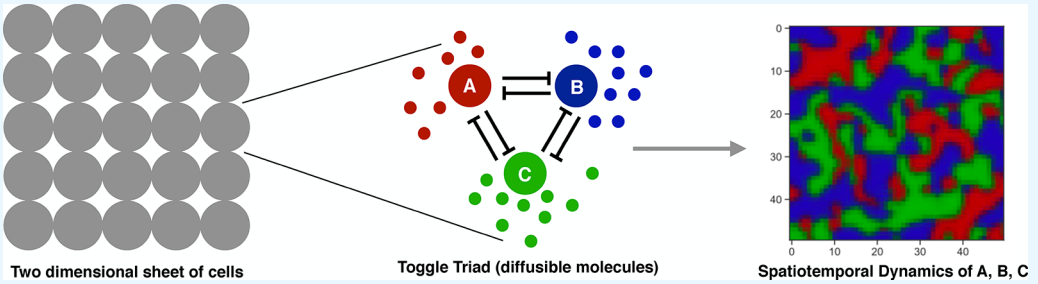

ABSTRACT: Spatiotemporal pattern formation plays a key role in various biological phenomena including embryogenesis and neural network formation. Though the reaction−diffusion systems enabling pattern formation have been studied phenomenologically, the biomolecular mechanisms behind these processes have not been modeled in detail. Here, we study the emergence of spatiotemporal patterns due to simple, synthetic and commonly observed two- and three-node gene regulatory network motifs coupled with their molecular diffusion in one- and two-dimensional space. We investigate the patterns formed due to the coupling of inherent multistable and oscillatory behavior of the toggle switch, toggle switch with double self-activation, toggle triad, and repressilator with the effect of spatial diffusion of these molecules. We probe multiple parameter regimes corresponding to different regions of stability (monostable, multistable, oscillatory) and assess the impact of varying diffusion coefficients. This analysis offers valuable insights into the design principles of pattern formation facilitated by these network motifs, and it suggests the mechanistic underpinnings of biological pattern formation.

INTRODUCTION

Pattern formation in living organisms is ubiquitous in nature, for instance, during embryonic development−[1] morphogenesis,[2] organization of neural networks,[3,4] and patterns on body (wing/skin/fur).[5] In smaller organisms, such as Hydra[6] and in the different species of *Drosophila*,[1] we observe emergence of patterns during formation of several structures. Some examples in higher organisms include wing decoration in butterfly, stripes in zebras, patches in giraffes or spots in leopards. These diverse patterns are often driven by morphogen gradients, and have been extensively investigated.[7−9] However, the underlying mechanisms in terms of gene regulatory networks are not as well-investigated. Thus, reproducing these patterns in synthetic biology has remained a challenging problem.

The theory of pattern formation was first explored mathematically in 1952 by Alan Turing in his seminal work.[10] In 1958, spontaneous, dynamic, and oscillating circular and spiral chemical patterns were first observed experimentally, famously known as, Belousov−Zhabotinsky (BZ) reactions.[11,12] In 1972, Gierer and Meinhardt[13] developed a theoretical model of the *Activator−Inhibitor system*, based on Turing's theory of 1952,[10] and also devised it experimentally.[14−16] In this two-component system an activator triggers the inhibitor while the inhibitor represses the activator in a long-range way. This mechanism could model different patterns including parallel stripes in shells, caused by near synchronous oscillations. Other theoretical models[17−19] also generate similar patterns thus, augmenting that mathematical models like Turing's drive development of theory for biological systems.[10]

Mathematical models incorporating diffusion of only one of the two components have already been developed.[20,21] Moreover, experiments have been designed in various contexts of a single diffusing molecule−[22,23] spatial arrangement and manipulation of inducers,[24,25] and quorum sensing molecules,[26,27] highlighting the importance of the Turing model in exploring pattern formation in many systems.[17−19] However, patterns emerging from diffusing molecules of gene regulatory networks is still in its formative stages, and there are many challenges to it.[28]

The inherent stochasticity due to spatial diffusion of molecules enhances the noise/fluctuations in the environment of a cell which can thus influence gene expression.[29] Molecular diffusion plays an important role in transcriptional regulation,

Received: July 22, 2022
Accepted: November 24, 2022
Published: January 17, 2023

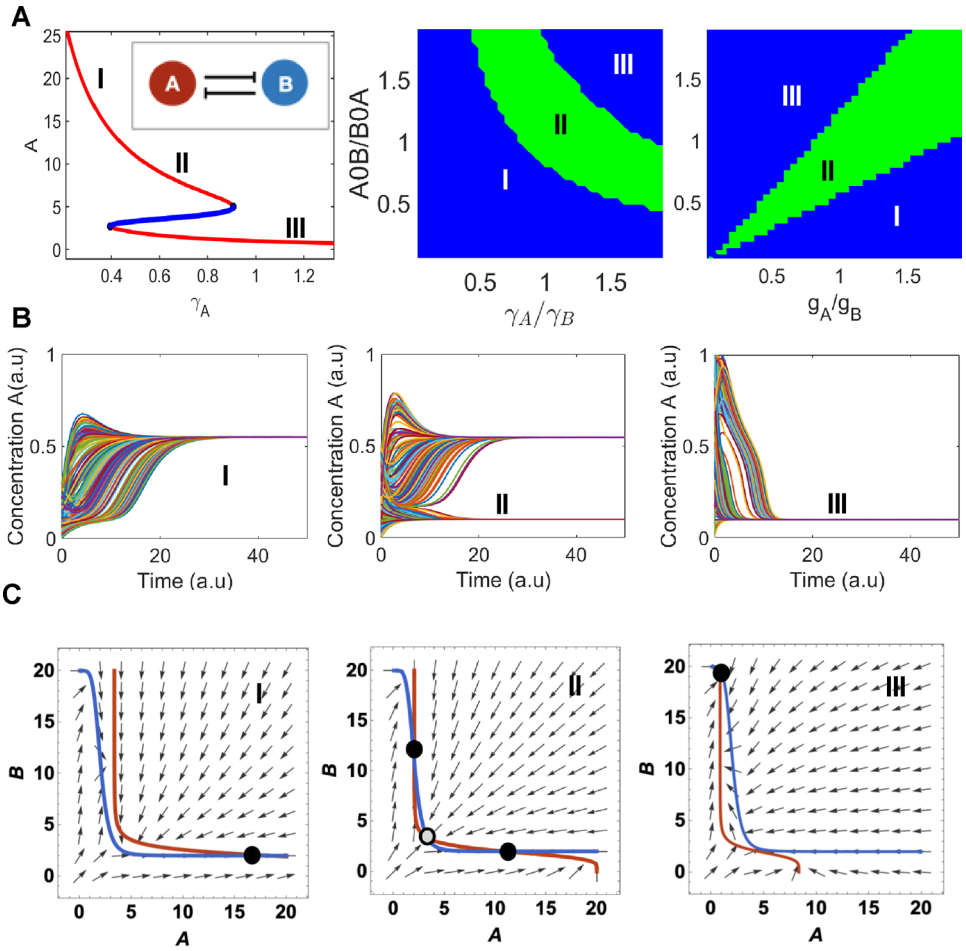

Figure 1. Temporal dynamics of toggle switch (TS): (A) Left: Bifurcation diagram of one of the proteins (A) as a function of degradation rate (γ_A) depicting the bistable behavior of a toggle switch (inset). Center and right: Phase diagrams between nondimensionalized parameters which control the strength of the toggle switch. Different colors depict different regions of bistability and monostability. A_0B/B_0A, γ_A/γ_B, and g_A/g_B are the ratio of thresholds, degradation rates, and production rates, respectively. (B) Time evolution of one of the proteins (A here) starting from different initial conditions under different regimes of bifurcation diagram. (C) Nullclines for different regimes of the parameter space. The black and gray circles denote stable and unstable fixed points of the system, respectively. The red curve is the plot for the solution of the first one of eq 1 at the steady state while the blue curve is the same for the second one of eq 1.

biochemical signaling etc.[30] Cottrell et al. developed an analytical model for branching-diffusion and estimated the mean and the magnitude of fluctuations which can be determined by the protein's Kuramoto length—the typical distance across which a protein can diffuse in its lifetime.[31] How such diffusion, coupled with emergent dynamics of the gene regulatory networks, can generate specific patterns is elusive and what we hope to contribute to.[28,32−34]

Here, we aim to study diverse patterns emerging out of spatiotemporal dynamics of interactive diffusive molecules of multiple simple two- and three-node gene regulatory network (GRN) motifs—toggle switch[35] with/without self-activation,[36] toggle triad,[37] and repressilator.[38] We have further observed how the patterns change corresponding to different stability regimes of a single motif and for varying diffusion coefficients. The patterns induced by GRNs are transient, evolve dynamically, and asymptotically reach a stable homogeneous state. The dynamics of pattern formation depend on the motif being investigated and operating regimes.

RESULTS

Toggle Switch—an Archetype of GRNs—Exhibiting Temporal and Spatial Bistability. We take a bottom-up approach and begin our study by analyzing the toggle switch, a network formed by two genes *A* and *B*, mutually repressing each other (schematic in the inset of the first plot of Figure 1 A). Each gene of *A* and *B* is usually a master regulator of a specific cellular fate and inhibits the activity of the other gene. It is an archetype of GRNs in various biological systems, for instance, mammalian cell fate tree (with toggle switch at each of its branch points).[39] Toggle switch enables two states: (high A, low B) which we call as state A and (low A and high B) which we call as state B. It displays both monostable and bistable behaviors at different parameter regimes. Such bistable behavior is exemplified in the above mentioned embryonic patterning of Drosophila[2,40] signaling networks[41] and galactose regulatory networks.[42,43]

The governing equation for genetic toggle switch—two genes mutually repressing each other—in terms of the shifted Hill function $\mathcal{H}$ is given by

https://doi.org/10.1021/acsomega.2c04581
ACS Omega 2023, 8, 3713−3725

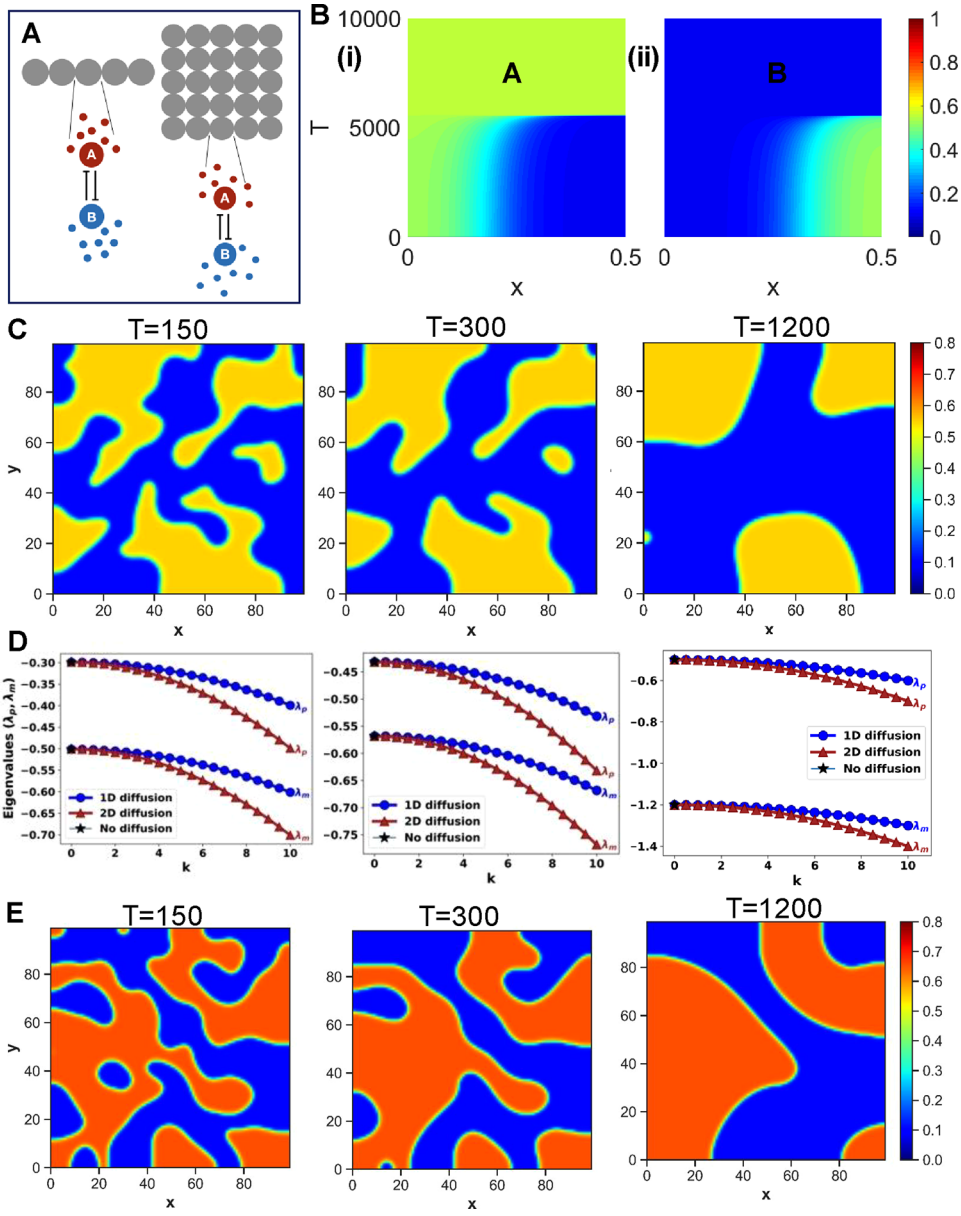

Figure 2. Spatiotemporal dynamics of the toggle switch (TS). (A) Schematic of toggle switch plus diffusion system. In the 1D system, we consider a single array of cells and each has a toggle switch with diffusive molecules. In the 2D system, we have a square lattice of cells. (B) Heatmaps of levels of protein A (i) and B (ii) as a function of time and space in the 1D diffusive system. (C) Heatmap of levels of A in the 2D diffusive system at different time points. (D) Analytical plots for the eigenvalues of TS (expressions in Supporting Information) in different parameter regimes, viz. Monostable-I (left), Bistable-II (center), and Monostable-III (right) (refer to previous figure). (E) Heatmaps of levels of A for another parameter set (Parameter set-2) at different time points..

$$\frac{dA}{dt} = f(A, B) = g_A \mathcal{H}(B, B_0A, n_{BA}, l_{BA}) - \gamma_A A$$
$$\frac{dB}{dt} = g(A, B) = g_B \mathcal{H}(A, A_0B, n_{AB}, l_{AB}) - \gamma_B B \quad (1)$$

where g_A and g_B are the production rates, γ_A and γ_B are the degradation rates. The first terms in the equations in (1) correspond to the effective production rates of the species and the second terms correspond to their degradation. The terms $\mathcal{H}(B, B_0A, n_{BA}, l_{BA})$ and $\mathcal{H}(A, A_0B, n_{AB}, l_{AB})$ are the shifted Hill functions and capture the interaction between gene A and gene B due to transcriptional inhibition.

$$\mathcal{H}(B, B_0A, n_{BA}, l_{BA}) = H_-(B, B_0A, n_{BA}, l_{BA}) + l_{BA}H_+(B, B_0A, n_{BA}, l_{BA}) = \frac{B_0A^{n_{BA}}}{B_0A^{n_{BA}} + B^{n_{BA}}} + l_{BA}\frac{B^{n_{BA}}}{B_0A^{n_{BA}} + B^{n_{BA}}}$$
$$\mathcal{H}(A, A_0B, n_{AB}, l_{AB}) = H_-(A, A_0B, n_{AB}, l_{AB}) + l_{AB}H_+(A, A_0B, n_{AB}, l_{AB}) = \frac{A_0B^{n_{AB}}}{A_0B^{n_{AB}} + A^{n_{AB}}} + l_{AB}\frac{A^{n_{AB}}}{A_0B^{n_{AB}} + A^{n_{AB}}} \quad (2)$$

https://doi.org/10.1021/acsomega.2c04581
ACS Omega 2023, 8, 3713−3725

In (2), B_0A and A_0B are the thresholds which determine the levels at which the transcriptional interaction becomes active. The Hill coefficients, n_{BA} and n_{AB}, correspond to the cooperativity of interaction and l_{BA} and l_{AB} are the fold changes in the levels of proteins due to transcriptional activation or inhibition. The fold change value of $l_{BA} > 1$ means that B is activating A and $l_{BA} < 1$ means that B is inhibiting A.[44]

First, we perform numerical analysis to understand the dynamical behavior of the toggle switch motif. Numerical bifurcation analysis shows that the system switches from a monostable region of only state A ((Ab) ≡ (high A, low B)) to a bistable region where both state A ((Ab) ≡ (high A, low B))) and state B ((aB) ≡ (low A, high B)) are permitted, to another monostable region with only state B ((aB) ≡ (low A, high B)) (see Figure 1A). Here capital letters denote high expression levels, while small letters denote low expression levels. The bifurcation parameter here is the degradation rate of A (γ_A). Starting from state A (region I), as we increase the degradation rate, the steady state concentration of A decreases and the system reaches a bistable region (region II), where the system can achieve both the states—A or B. If we further increase the degradation rate of A, the system can only attain state B (where B is high and A is low). The opposite behavior can be seen if the degradation rate of B is chosen as a bifurcation parameter (Figure S1 B).

Next, we draw the phase diagram depicting the stability regions. On the y-axis, we have $A0B/B0A$, and as we increase this ratio, the relative strength of inhibition of A on B, as compared to B on A, decreases. In the first phase diagram, we have the ratio of their degradation rates (γ_A/γ_B) on the x-axis. As this ratio increases, the inhibition strength by A decreases. Therefore, the region marked I is the region where we observe state A, and in region II, the inhibition of both A and B are balanced and we observe a bistable behavior. In the region III, the inhibition of A on B is weak as compared to B′S inhibition on A; therefore we observe the state B (high B, low A Ba)

Next, we numerically solved the eqs 1 starting from 200 different initial conditions and from parameters in different regions. Dynamics of the corresponding region reveal the system converging to one or both states (Figure 1B). The dynamics of B are presented in Figure S1A,B.

Panel C depicts the nullclines for the three regimes having one, two, and one stable fixed points marked by solid black circles. The unstable steady state is shown by gray circle. The red curve is the plot for the solution of the first one of eq 1 in the steady state while the blue curve is the same for the second one of eq 1. The arrows represent the vector fields. They are directed toward the stable fixed point and away from the unstable one. A monostable regime is signified by having a single stable steady state or cells having one phenotype while a bistable regime signifies the possibility of a population of cells having two different fates denoted by two stable steady states. The bistable temporal dynamics of gene B for parameter set 1 corresponding to three stability regimes (same as in Figure 1) and its bifurcation diagram, the phase diagrams (ratio of thresholds as a function of ratios of production rates and degradation rates respectively) and nullclines for parameter sets 2 and 3 are shown in Figure S1D. Phase diagrams of the time taken for gene A to reach the steady state are also presented in the Figure S2A−C.

Toggle Switch with 1D Diffusion. Tkacik and Bialek developed a mathematical model for understanding the one-dimensional diffusion—longitudinal sliding of repressor molecules along DNA during transcriptional regulation.[30] Here, we consider a one-dimensional chain of cells (depicting hair-line/filamentous structures), each having a toggle switch with diffusing molecules of gene products (see Figure 2A for the schematic). Each molecule can diffuse through the entire one-dimensional space. The mathematical equations describing the system can be written in the following way,

$$\frac{dA}{dt} = g_A \mathcal{H}(B, B_0A, n_{BA}, l_{BA}) - \gamma_A A + D_A \frac{\partial^2 A}{\partial x^2}$$

$$\frac{dB}{dt} = g_B \mathcal{H}(A, A_0B, n_{AB}, l_{AB}) - \gamma_B B + D_B \frac{\partial^2 B}{\partial x^2} \quad (3)$$

The above equations are similar to eq 1 with one added term in the right-hand side describing diffusion. D_A and D_B are the diffusion constants/diffusivities for genes A and B. Higher diffusivity means faster diffusion. $\partial^2A/\partial x^2$ and $\partial^2B/\partial x^2$ capture the spatial dependencies/evolution/fluxes of the concentration of gene products A and B respectively. Figure 2B shows bistable spatiotemporal behavior of toggle switches with molecules diffusing in one-dimensional space. Green and blue represent the higher and the lower expression levels of gene A. The simulation starts with a spatially in-homogeneous state (having both expression levels) but as time progresses, the system reaches its steady homogeneous state. One can notice the complementary behavior of (i) gene A and (ii) gene B as expected from a toggle switch.

Toggle Switch with 2D Diffusion. Consider a two-dimensional square lattice of cells (depicting a thin monolayer of biological tissue), each cell having a toggle switch with diffusing gene molecules (see Figure 2A for the schematic). Each molecule can diffuse through the entire two-dimensional space.

$$\frac{dA}{dt} = g_A \mathcal{H}(B, B_0A, n_{BA}, l_{BA}) - \gamma_A A + D_A^x \frac{\partial^2 A}{\partial x^2} + D_A^y \frac{\partial^2 A}{\partial y^2}$$

$$\frac{dB}{dt} = g_B \mathcal{H}(A, A_0B, n_{AB}, l_{AB}) - \gamma_B B + D_B^x \frac{\partial^2 B}{\partial x^2} + D_B^y \frac{\partial^2 B}{\partial y^2} \quad (4)$$

In two dimensions, the equations have two added terms in the right-hand side describing diffusion in two different directions. D_A^x, D_A^y and D_B^x, D_B^y are the diffusion constants/diffusivities for genes A and B in the x- and y-directions, respectively.

The spatiotemporal behavior of toggle switches with molecules diffusing in two-dimensional space at three different time instants is shown in Figure 2C. We notice that as time progresses, the arbitrary-shaped yellow patches become regular, and the state represented by blue gradually wins over (Supporting Video S3.1). Panel D shows analytical plots for eigenvalues in different parameter regimes, viz. I-Monostable, II-Bistable, and III-Monostable. Analytical solutions reveal negative eigenvalues, thus indicating the steadiness of the patterns. With the increase in wavenumber k, eigenvalues become more negative. For $k = 0$, the system reduces to the diffusion-free case. In two dimensions, the fast convergence to the patterns, seen across multiple parameter sets, strengthen the stability and robustness of observed patterns. We also conducted similar analyses for another parameter set (Figure 2E) and found that the patterns are qualitatively similar. The nature of the stability of these dynamical systems can be evaluated from the trace, determinant, and eigenvalues of the linear stability matrix. The detailed calculation, in general (not particular to any specific motifs), is in Section 1.1 in Supporting Information. The

https://doi.org/10.1021/acsomega.2c04581
ACS Omega 2023, 8, 3713−3725

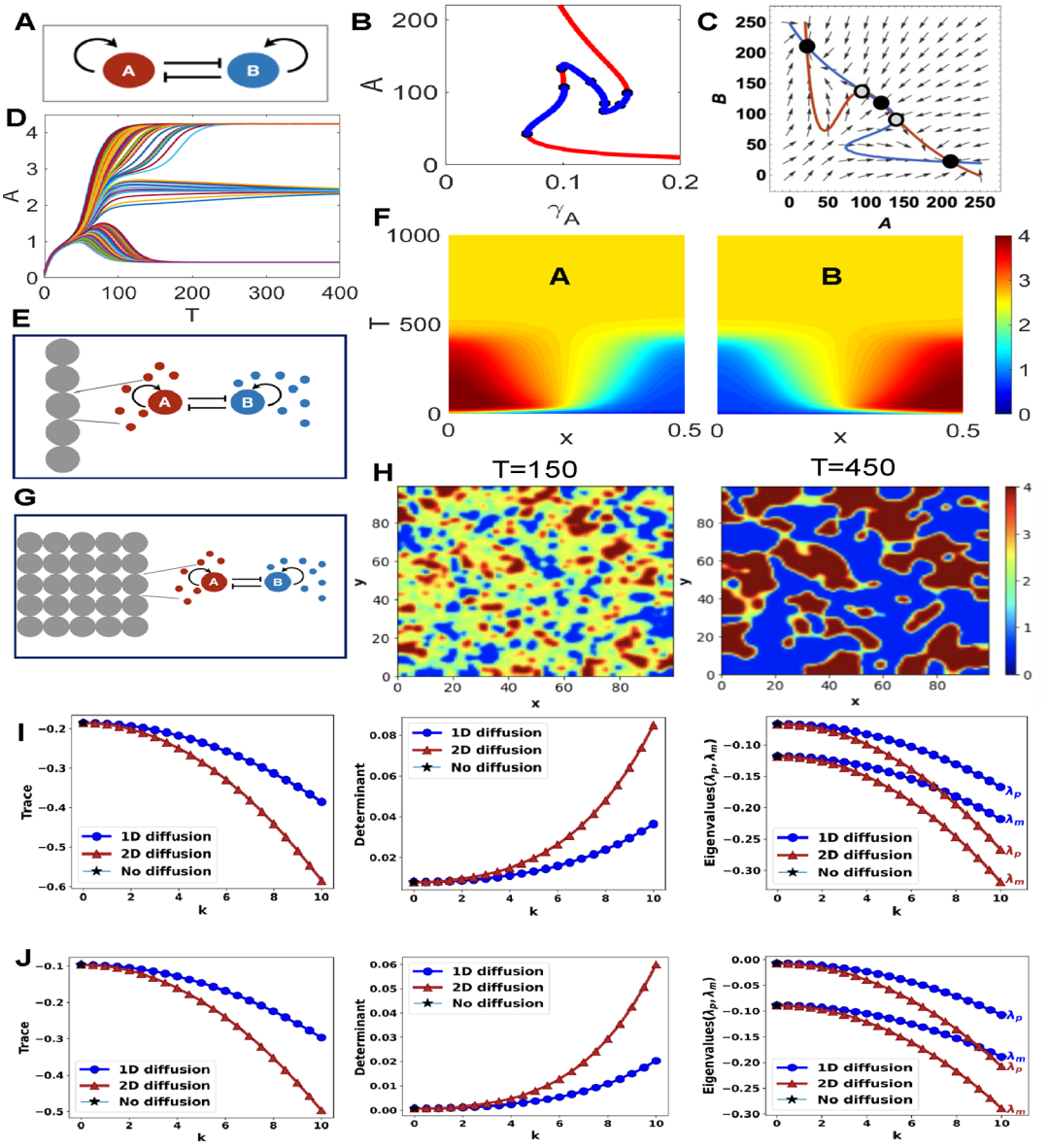

Figure 3. Dynamics of toggle switch with self-activation (TSSA). (A) Schematic of the ODE model. (B) Bifurcation diagram of A as a function of degradation rate of A. Note the presence of a tristable region. (C) Nullcline plot of the tristable region. The black and gray circles denote stable and unstable fixed points of the system, respectively. (D) Time evolution plot of protein A for multiple initial conditions in the tristable parameter regime. (E) Schematic of the TSSA coupled with the 1D diffusive system. (F) Heatmap of levels of A and B as a function of space and time for parameter set A. (G) Schematic of the TSSA coupled with the 2D diffusive system. (H) Heatmaps of levels of A for parameter set 1 at two different time points. (I) Trace, determinants, and eigenvalues evaluated at equilibrium points 1 and 3. (J) Trace, determinants, and eigenvalues evaluated at equilibrium points 2.

calculation and the expressions for eigenvalues for each of the motifs are given in subsequent sections in the Supporting Information. The stability (quantified by the nature of trace, determinant and eigenvalues) of the patterns in one-dimension is similar and robust across parameters (shown for parameter sets 1, 2, and 3 in Figures S3A−C and S4A−C).

Toggle Switch with Self-Activation—Exhibiting Spatiotemporal Tristability. The next motif we consider is two self-activation loops coupled with a toggle switch (TSSA) (see Figure 3A). This architecture introduces a third stable steady state in the system. The balance between mutual repression and double self-activation enhances the probability of having a third state (intermediate A−intermediate B) in addition to the two possibilities of expression levels of toggle switch (high A−low B) and (low A−high B).[36,37,45,46] The additional third/hybrid stable steady state starts emerging as the strength of the self-activation loops are increased. Weak self-activation reduces TSSA to a simple toggle switch. Further enhancement of the strengths of the links stabilizes the hybrid state while destabilizing the two canonical stable steady states.[36] Emergence of the stable hybrid state enabled by self-activations in toggle switch has been observed in different biological phenomena of cellular decision making. A few examples include (i) branching of multipotent progenitor cells into erythroid and myelomonocytic lineages governed by two key transcription factors—GATA1 and PU.1,[47] (ii) epithelial-to-mesenchymal transition (a key regulatory process involving transcription factors ZEB/SNAIL and microRNAs miR34/miR200) during embryogenesis, wound healing, and cancer progression,[48−50] and (iii) stabilization of hybrid T-helper cells having properties of both

https://doi.org/10.1021/acsomega.2c04581
ACS Omega 2023, 8, 3713−3725

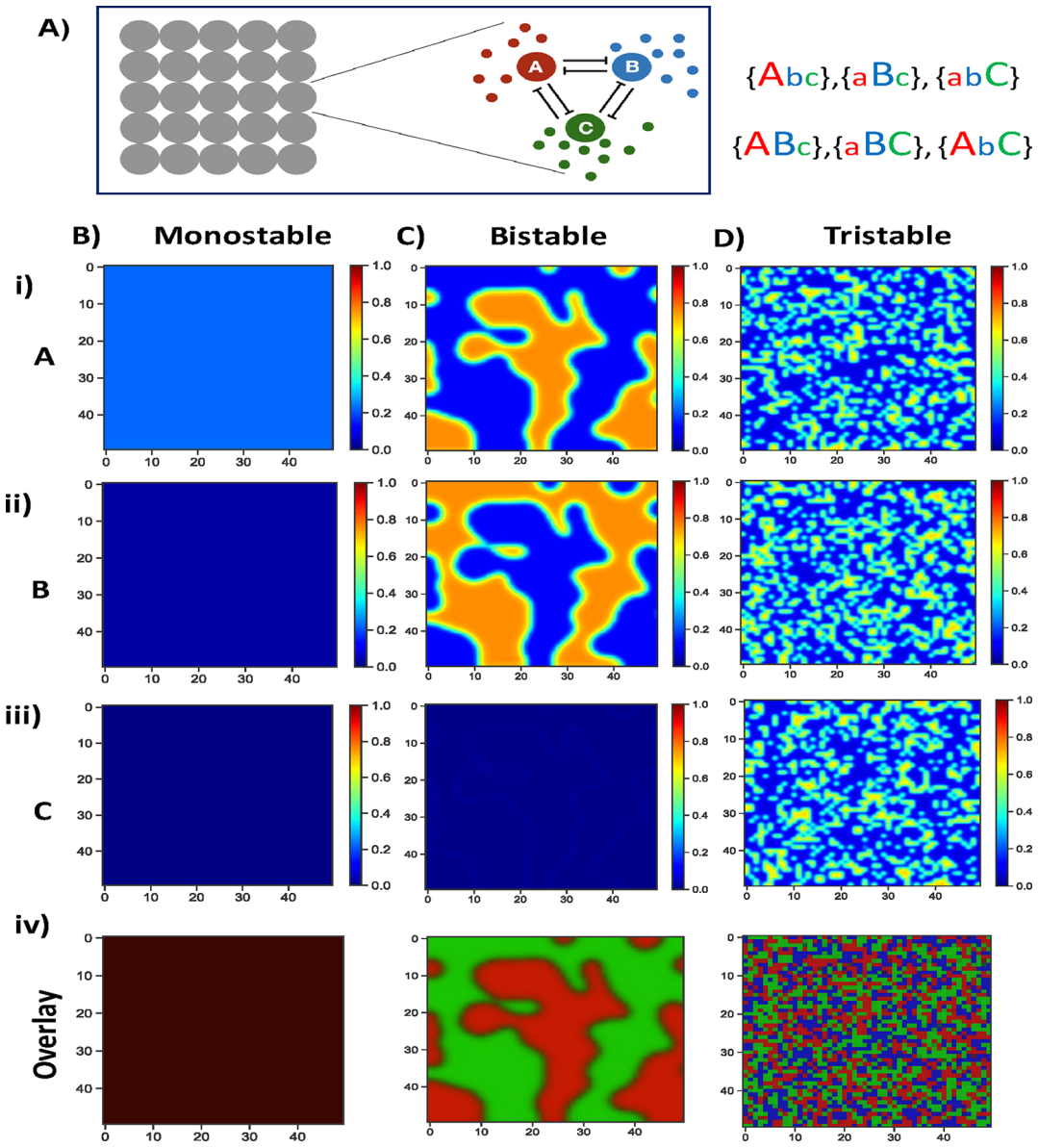

Figure 4. Dynamics of toggle triad. (A) Schematic of toggle triad of three species in a cell coupled with the diffusion system. (B) Heat map of levels of (i) A, (ii) B, and (iii) C as a function of space in the monostable parameter regime. Protein A is high in all cells as compared to B and C. (iv) RGB (red green blue) plot of the three species combined. Here, red corresponds to high A, green corresponds to high B, and blue corresponds to high C. (C) Same as part B for the bistable parameter regime where either A is high or B is high. (D) Same as part B) but for tristable parameter regime in which either A is high or B is high or C is high.

Th1/Th2 cells during lineage specification.[51] The governing mathematical equations for such a system is given by

$$\frac{dA}{dt} = g_A \mathcal{H}(B, B_0A, n_{BA}, l_{BA})\mathcal{H}(B, A_0A, n_{AA}, l_{AA}) - \gamma_A A$$
$$\frac{dB}{dt} = g_B \mathcal{H}(A, A_0B, n_{AB}, l_{AB})\mathcal{H}(A, B_0B, n_{BB}, l_{BB}) - \gamma_B B \quad (5)$$

where $\mathcal{H}(B, B_0A, n_{BA}, l_{BA})$ and $\mathcal{H}(A, A_0B, n_{AB}, l_{AB})$ are the shifted Hill functions as given in eq 2 in the previous section, while the other two shifted Hill functions are for the self-loops, given by the following,

$$\mathcal{H}(B, A_0A, n_{AA}, l_{AA}) = H\_(B, A_0A, n_{AA}, l_{AA}) + l_{AA}H_+(B, A_0A, n_{AA}, l_{AA}) = \frac{A_0A^{n_{AA}}}{A_0A^{n_{AA}} + \nu^{n_{AA}}} + l_{AA}\frac{\nu^{n_{AA}}}{A_0A^{n_{AA}} + \nu^{n_{AA}}}$$
$$\mathcal{H}(A, B_0B, n_{BB}, l_{BB}) = H\_(A, B_0B, n_{BB}, l_{BB}) + l_{BB}H_+(A, B_0B, n_{BB}, l_{BB}) = \frac{B_0B^{n_{BB}}}{B_0B^{n_{BB}} + A^{n_{BB}}} + l_{BB}\frac{u^{n_{BB}}}{B_0B^{n_{BB}} + A^{n_{BB}}} \quad (6)$$

Figure 3B shows the bifurcation diagram of A. The expression levels of A is shown as a function of degradation rate of A, γ_A. The three stable states are shown in red, while the two unstable

https://doi.org/10.1021/acsomega.2c04581
ACS Omega 2023, 8, 3713−3725

states are shown in blue. The corresponding nullclines are shown in (Figure 3 C). The three stable fixed points are marked by solid black circles while the two unstable steady states are shown by gray circles. (Figure 3D) shows the time evolution of gene A for 200 different initial conditions, finally all ending up in three different stable steady states.

Toggle Switch with Self-Activation with 1D Diffusion. Let us now consider a one-dimensional chain of cells (depicting hair-line/filamentous structures), each having a toggle switch coupled with two self-activation loops (TSSA) (schematic in Figure 3E). Each molecule can diffuse through the entire one-dimensional space. The governing equations are

$$\frac{dA}{dt} = g_A \mathcal{H}(B, B_0A, n_{BA}, l_{BA})\mathcal{H}(B, A_0A, n_{AA}, l_{AA}) - \gamma_A A + D_A \frac{\partial^2 A}{\partial x^2}$$

$$\frac{dB}{dt} = g_B \mathcal{H}(A, A_0B, n_{AB}, l_{AB})\mathcal{H}(A, B_0B, n_{BB}, l_{BB}) - \gamma_B B + D_B \frac{\partial^2 B}{\partial x^2} \quad (7)$$

where $\mathcal{H}$ are the shifted Hill functions as described in the previous sections and the last two terms in the RHS describe molecular diffusion (D_A and D_B being the diffusion coefficients of A and B, respectively). Figure 3F shows the heat map of expression levels of A and B as a function of space and time for parameter set A. The complementarity natures in expression levels of gene A and gene B are shown side by side for comparison.

Toggle Switch with Self-Activation with 2D Diffusion. Consider a two-dimensional square lattice of cells (depicting thin monolayer of biological tissue), each having a toggle switch coupled with two self-activation loops (TSSA) (Figure 3G). Each molecule can diffuse through the entire two-dimensional space. The mathematical equations describing the scenario are given by

$$\frac{dA}{dt} = g_A \mathcal{H}(B, B_0A, n_{BA}, l_{BA})\mathcal{H}(B, A_0A, n_{AA}, l_{AA}) - \gamma_A A + D_A^x \frac{\partial^2 A}{\partial x^2} + D_A^y \frac{\partial^2 A}{\partial y^2}$$

$$\frac{dB}{dt} = g_B \mathcal{H}(A, A_0B, n_{AB}, l_{AB})\mathcal{H}(A, B_0B, n_{BB}, l_{BB}) - \gamma_B B + D_B \frac{\partial^2 B}{\partial x^2} + D_B^y \frac{\partial^2 B}{\partial y^2} \quad (8)$$

where the shifted Hill functions are expressed same as in the previous section, and there are two diffusive terms (in x- and y-spatial directions) for each gene.

Figure 3H shows the heatmaps of levels of gene A for parameter set 1 at two different time points for TSSA with molecules diffusing in two-dimensional space. We observe three states in the initial time point (T = 150) A being high, intermediate or low. As time progresses and molecules diffuse, the intermediate state vanishes and A-high or A low dominate. (Supporting Video S3.2). In Figure 3I, we show the analytical plots for the trace, determinants, and eigenvalues of the linear stability matrix, evaluated at equilibrium points 1 (we obtain exactly same results as obtained at the second equilibrium point since the coordinates of equilibria are symmetric), and panel J shows the same quantities evaluated at equilibrium points 2. The temporal evolution and the spatiotemporal dynamics corresponding to the tristable parameter regime is also shown here. Additionally, we solved the system in a bistable parameter regime and studied the steady states and spatiotemporal dynamics (Figure S5A−G). The overall behavior is similar to that of the bistable regime in toggle switch.

Toggle Triad—a Frustrated Tristable System. We consider a toggle triad, three coupled toggle switches, comprising the genes A, B, and C mutually repressing each other (schematic shown in Figure 4 A). This motif can have "pure"/single positive (A-high, B-low, C-low {Abc} or A-low, B-high, C-low {aBc} or A-low, B-low, C-high {abC}), "hybrid"/double positive (A-high, B-high, C-low {ABc} or A-low, B-high, C-high {aBC} or A-high, B-low, C-high {AbC}), or triple positive (A-high, B-high, C-high {ABC}) and triple negative (A-low, B-low, C-low {abc}) states. In our previous study,[37] we showed that the frequency of triple positive and triple negative states is very low. Single positive states are more frequent compared to the double positive states. It should be noted that toggle triad is a frustrated system;[52] e.g., high levels of A will drive levels of B to be low by repressing it, and low levels of B will make levels of C higher, which will eventually reduce the levels of A.

$$\frac{d\mathbf{A}}{dt} = f(\mathbf{A}, \mathbf{B}, \mathbf{C}) = \mathcal{H}(\mathbf{B}, B_0A, n_{BA}, l_{BA})\mathcal{H}(\mathbf{C}, C_0A, n_{CA}, l_{CA}) - \gamma_A \mathbf{A}$$

$$\frac{d\mathbf{B}}{dt} = g(\mathbf{A}, \mathbf{B}, \mathbf{C}) = \mathcal{H}(\mathbf{C}, C_0B, n_{CB}, l_{CB})\mathcal{H}(\mathbf{A}, A_0B, n_{AB}, l_{AB}) - \gamma_B \mathbf{B}$$

$$\frac{d\mathbf{C}}{dt} = h(\mathbf{A}, \mathbf{B}, \mathbf{C}) = \mathcal{H}(\mathbf{A}, A_0C, n_{AC}, l_{AC})\mathcal{H}(\mathbf{B}, B_0C, n_{BC}, l_{BC}) - \gamma_C \mathbf{C} \quad (9)$$

where $\mathcal{H}$ are the shifted Hill functions defined as in the previous sections with different arguments which can be obtained by systematic changes. Here we focus on monostability, bistability, and tristability of single positive states since they are most frequent. The patterns formed by double-positive states are also not significantly different from the single-positive ones.

Toggle Triad with 2D Diffusion. To study the pattern formation due to toggle triad, we coupled the motifs into the 2D lattice of cells. We write reaction−diffusion equations as follows:

https://doi.org/10.1021/acsomega.2c04581
ACS Omega 2023, 8, 3713−3725

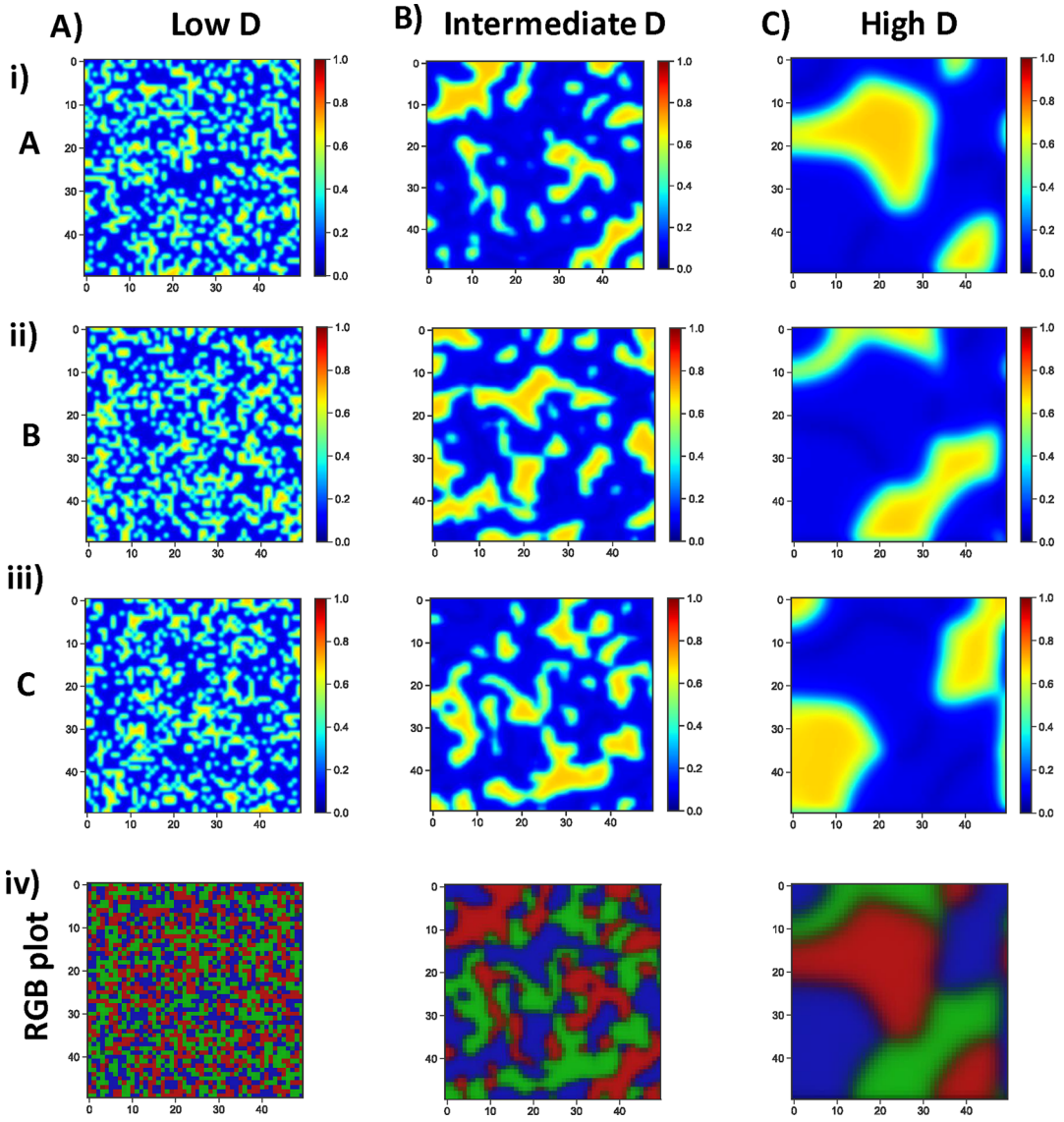

Figure 5. Dynamics of toggle triad in the tristable parameter regime for different diffusion constants. (A) Heat map of levels of (i) A, (ii) B, and (iii) C as a function of space in the tristable parameter regime when the diffusion is low ($D = 0.0008$). (iv) RGB plot of the three species combined. Here, red corresponds to A high, green corresponds to B high, and blue corresponds to C high. (B) Same as part A but for intermediate diffusion levels ($D = 0.008$). (C) Same as part A but for high diffusion levels ($D = 0.08$).

$$\frac{d\mathbf{A}}{dt} = \mathcal{H}(\mathbf{B}, B_0A, n_{BA}, l_{BA})\mathcal{H}(\mathbf{C}, C_0A, n_{CA}, l_{CA}) - \gamma_A\mathbf{A} + D_A^x\frac{\partial^2\mathbf{A}}{\partial x^2} + D_A^y\frac{\partial^2\mathbf{A}}{\partial y^2}$$

$$\frac{d\mathbf{B}}{dt} = \mathcal{H}(\mathbf{C}, C_0B, n_{CB}, l_{CB})\mathcal{H}(\mathbf{A}, A_0B, n_{AB}, l_{AB}) - \gamma_B\mathbf{B} + D_B^x\frac{\partial^2\mathbf{B}}{\partial x^2} + D_B^y\frac{\partial^2B}{\partial y^2}$$

$$\frac{d\mathbf{C}}{dt} = \mathcal{H}(\mathbf{A}, A_0C, n_{AC}, l_{AC})\mathcal{H}(\mathbf{B}, B_0C, n_{BC}, l_{BC}) - \gamma_C\mathbf{C} + D_C^x\frac{\partial^2\mathbf{C}}{\partial x^2} + D_C^y\frac{\partial^2\mathbf{C}}{\partial y^2} \quad (10)$$

We first explore the evolving patterns in different phases, i.e., monostable, bistable, and tristable. When the motif shows the monostable behavior (here A-high, B-low, and C-low {Abc}), the system reaches a homogeneous state (Figure 4B), as expected. When the motif is in the bistable parameter regime (here {Abc}-{aBc}), we get domains of regions where A is high and others where B is high. C remains low in all regions (Figure 4C). In the tristable parameter regime (here {Abc}-{aBc{abC}), we see pattern formation in all three species. The 2D space is distributed into different regions where either A is high or B is high or C is high. From the overlay plot is clear that only one of the genes is high in each cell (Figure 4D), reflecting patterns seen in the toggle triad (Supporting Video S3.3).

Next, we studied the role of diffusion constant on the pattern formation. In the tristable parameter regime, when the diffusion constant is low ($D = 0.0008$), we observe that the size of the yellow patches corresponding to the regions where either of the three states (Abc, aBc, or abC) is small (Figure 5A) as compared to the case where the diffusion constant is intermediate ($D = 0.008$) (Figure 5B which is same as Figure 4D). As the diffusion constant increases ($D = 0.08$), the yellow patch size of the

https://doi.org/10.1021/acsomega.2c04581
ACS Omega 2023, 8, 3713−3725

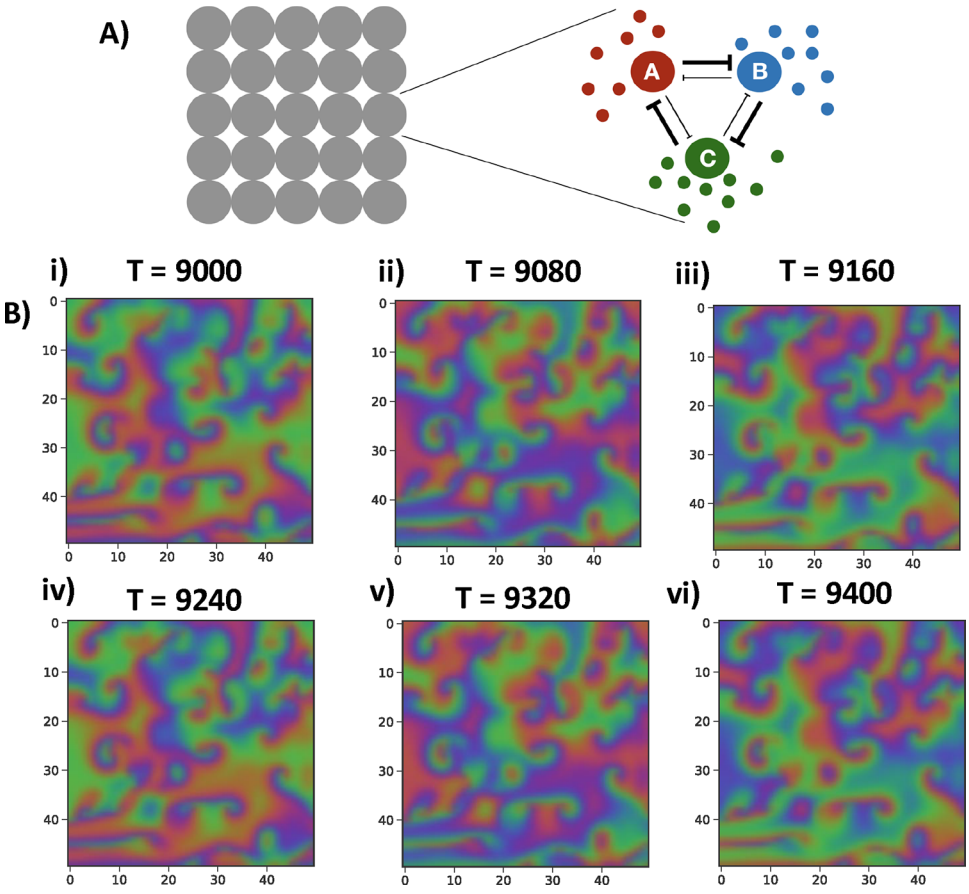

Figure 6. Repressilator as a special case of toggle triad. (A) Schematic of repressilator as a special case of toggle triad of three species in a cell, coupled with the diffusion system. One cycle of the repression is weak as compared to the other one. (B) An RGB (red-green-blue) plot of levels of A, B, and C, respectively, at six different time-points: (i) T = 9000, (ii) T = 9080, (iii) T = 9160, (iv) T = 9240, (v) T = 9320, and (vi) T = 9400.

patterns increases (Figure 5C). Diffusion enables the regions of stability to coalesce.

We also studied the effect of variable diffusion on pattern formation from a toggle triad motif in the bistable regime (see Figure S6A−C of the Supporting Information).

Time evolution (panels A and C) of the molecules of gene A for multiple initial conditions and the frequency distributions (panel B and D) of different states at steady state in the bistable and tristable parameter regimes of toggle triad is shown in Figure S7. Similarly, as in the cases for previous motifs, the stabilities of the patterns are quantified by traces, determinants, and three eigenvalues of linear stability matrix for different stability (mono (Figure S8), bi (Figure S9) and tri (Figure S10)) regimes and for low (panel A) and high (panel B) diffusivity.

Repressilator—Showcasing Spatiotemporal Oscillations. Oscillatory/rhythmic behaviors in biological systems are often generated by the complex interactions among various genes, proteins, metabolites etc. A number of factors like negative feedback, time delay, or inherent nonlinearity of the reaction kinetics can give rise to biochemical oscillations.[53] Elowitz and Leibler[38] first designed and constructed an artificial biological clock, called repressilator, with three transcription factors in *Escherichia coli*.

By weakening three links of the toggle triad (see schematic in (Figure 6A) through the corresponding parameter set in the excel sheet), we obtain the motif for repressilator genes, with *A*, *B*, and *C* repressing each other sequentially and cyclically. This is a well-known example of a biological oscillator. We have obtained repressilator as a limiting case of toggle triad by weakening specific links which behaves functionally as a "standard" repressilator. A toggle triad consists of the following 6 links: (a) A inhibits B, (b) B inhibits C, (c) C inhibits A, (d) A inhibits C, (e) C inhibits B, and (f) B inhibits A. If we weaken the strength of links d−f while maintaining the a−c ones (or vice versa), we get a standard repressilator. The governing equations are given by

$$\begin{aligned}\frac{d\mathbf{A}}{dt} &= \mathcal{H}(\mathbf{B}, B_0A, n_{BA}, l_{BA})\mathcal{H}(\mathbf{C}, C_0A, n_{CA}, l_{CA}) - \gamma_A\mathbf{A}\\ \frac{d\mathbf{B}}{dt} &= \mathcal{H}(\mathbf{C}, C_0B, n_{CB}, l_{CB})\mathcal{H}(\mathbf{A}, A_0B, n_{AB}, l_{AB}) - \gamma_B\mathbf{B}\\ \frac{d\mathbf{C}}{dt} &= \mathcal{H}(\mathbf{A}, A_0C, n_{AC}, l_{AC})\mathcal{H}(\mathbf{B}, B_0C, n_{BC}, l_{BC}) - \gamma_C\mathbf{C}\end{aligned} \tag{11}$$

We observe interesting dynamics when we couple the repressilator motif with the diffusion dynamics. Initially the system develops dynamic patterns which do not repeat themselves. After a time point (around T = 8500 here), they start repeating themselves. Although the molecules diffuse throughout the space the pattern repeats itself every 240 time steps. We also observe the formation of localized spirals serving as epicenters of spirals − a repeating motif (Figure 6B(i−vi)). A video of the oscillatory patterns is presented in the Supporting Information, Video S3.4. The overlay plot is shown in the main while the separate expression levels for the molecules of gene A,

https://doi.org/10.1021/acsomega.2c04581
ACS Omega 2023, 8, 3713−3725

gene B, and C for the same parameter set are shown in Figure S11. The oscillatory behavior is shown from the analytical calculation and its graphical representation of the three eigenvalues (one positive, and two complex eigenvalues with negative real component) for diffusion in two-dimensional space as a function of the wavenumber k in Figure S12.

DISCUSSION

Many biological phenomena result from a constant tug-of-war between the contrasting aspects of stochastic and deterministic behavior, i.e., random fluctuations in gene expression, concentration of numerous intracellular biomolecules, and their interactions via different signaling pathways, cell-to-cell variability, intercellular communication, etc., ultimately resulting in some coordinated emergent phenomena of cellular division, differentiation, and development.[54] Similarly, for the biological systems which fall into the category of reaction−diffusion systems, biochemical "reactions" are a stabilizing/homogenizing/equilibrating process while molecular "diffusion" is trying to destabilize it. These two contradictory processes result in the spontaneous emergence of spatiotemporal patterns. "Reaction" and "diffusion" might refer to intracellular biochemical reactions and intercellular signaling/communication (at the tissue-level) respectively. Unraveling the underlying mechanisms of these processes is one of the key challenging problems in synthetic[28] and developmental biology. An asymptotically stable homogeneous steady-state of an inherently nonlinear system becoming unstable by the effect of self- and/or cross-diffusion is known as diffusion-driven instability or Turing instability.[55]

Spatiotemporal patterns have been studied in multifarious contexts with different length-scales and time-scales. In population ecology—the systems of interacting population of prey-dependent predator−prey models with the influence of self- and cross-diffusion, gestation delays, and weak allele effects—analyzing formation of different patterns is an interesting domain of study.[56−59] Bacterial pattern formation[60] has been studied to understand the effects of biofilms and quorum-sensing in pathogenic bacteria *Staphylococcus aureus*,[61] and *E. coli*[62,63] by simulating their gene regulatory systems.

Many theoretical[64−68] and experimental[69−71] studies suggest that the reaction−diffusion mechanism plays the primary role in producing patterns (stripes, spots, patches, and color variations) on animals, birds, insects, and fish. Using fluorescence microscopy and in situ hybridization techniques, Fritsch et al.[72] observed beautiful expression patterns of gap and pair-rule genes such as hunchback and bicoid in *Drosophila* embryo. These gene networks spatial bistability.[2]

Barbier et al. constructed synthetic toggle switches in*E. coli*and maintained them under the influence of diffusive gradients of an external inducer and regulator and observed, characterized, and tuned spatiotemporal patterning exhibiting bistability and hysteresis.[32] Besides naturally existing patterns, synthetic patterns have been engineered in microbial communities.[60,73] Theoretical explorations of spatial patterns (transient but persistent) formed from quorum-sensing modules of bistable toggle switch and a four-state GRN with diffusible molecules in one- and two-dimensional space, having leaky gene expression and cross-talk,[62] is also worth mentioning. Quite recently Tompkins et al. performed quantitative analysis of Turing's hypothesis and experimental testing of it on an emulsion of aqueous droplets (mimicking a circular array of cells).[74] This also opens up applications of the Turing model in material science. Though there have been a plethora of theoretical explorations on biological pattern formation over decades, studies of these in the context of gene regulatory networks is a very recent paradigm of interest.

We have presented a detailed analysis of spatiotemporal patterns emerging from the spatially cued molecules involved in two- and three-node regulatory networks showing multistability or oscillatory behavior. The analysis begins with the simple two-node network of toggle switch, having both monostable and bistable behavior. Toggle switch coupled with self-loops yields an additional stable state. Toggle triad is the next example which shows all the mono-, bi-, and tristable behaviors in the spatiotemporal dynamics. Finally, the Repressilator network exhibits an oscillatory behavior. The time period of the spatiotemporal oscillations can be varied significantly by changing the rate of degradation of the gene-products (see Figure S12).

The full nonlinear model should be solved to gain more precise and detailed insights instead of Linear Stability Analysis. The latter has captured a majority of the dynamical features of the system qualitatively, leaving out some of the intricate details. We have developed a generic, and coarse-grained, but strong, theory which has the potential to capture various spatiotemporal patterns by taking into account the structure and parameter regimes of the underlying gene regulatory networks.

In simulations, we assumed free diffusion across cell membranes. In real biological systems, the positional and structural information about the cell-membranes and organelles is required to set up the diffusion gradient. Visually similar *in-silico* patterns can be generated from equations having different reaction and diffusion terms. Thus, an interplay of more than one factor can occur to bring about a biological stationary pattern. *In-silico*, ordered spatiotemporal patterns such as stripes and spots, can also be formed within this mathematical framework. We illustrate different mechanisms, from special initial conditions, generating the striped patterns in toggle triad and spotted patterns from spatially-varying diffusion coefficient in toggle switch (see Figure S14 for reference).

Animals can have different body structures, sizes, shapes, and curvatures which demand tackling of the nonlinear multivariate system of partial differential equations, to be solved for different geometries/topologies—spherical, cylindrical, etc. For simplicity, we have taken diffusion coefficient for different genes to be the same. Realistically, these should differ inherently and along different directions and might be a function of space due to anisotropy in diffusion of molecules. Thus, next steps include incorporating these realistic features and different initial and boundary conditions imitating more realistic biological scenarios. The systems can be studied for more specific biological cases where we can tune parameters using experimental results. In our analysis, we have diagonal diffusivity tensors, as we have only self-diffusion of the biomolecules. This assumption is reasonable because molecular diffusion of one molecule does not depend directly on others. We can extend to these scenarios and tackle more realistic cases which will have nonzero off-diagonal elements in the diffusivity tensor to capture the cross-diffusion dependence on perhaps the concentration gradient of some external component (inducer and/or regulator). Here, we have analyzed bivariate (toggle switch) and trivariate systems (toggle triad and repressilator). In principle, systems can be in general be multivariate (toggle polygons and other networks) described by multiple nonlinear coupled partial differential equations. The essence of the

https://doi.org/10.1021/acsomega.2c04581
ACS Omega 2023, 8, 3713−3725

problem remains the same, while the complexity of solving it increases multifold due to a larger number of parameters.

Despite providing valuable insights into the emergent dynamics of pattern formation, our analysis here has multiple limitations. First, we have modeled reaction−diffusion systems, i.e., added a diffusive term in the PDEs describing the evolutionary dynamics of the motifs. We do not consider the length and time scales explicitly in our problem, since these scales are implicitly present in the diffusion coefficient term. Considering diffusion-limited biomolecular reaction kinetics (rate of reactions being functions of the diffusive transport of molecules) is important in some scenarios.[75] Second, we have considered a static lattice with fixed domain in our simulations. Cell division and death (apoptosis/necrosis) is not relevant in the time scales we are considering. Third, transcription factors are not known to diffuse across cell membranes. The molecules considered here are not necessarily transcription factors but can represent, at a coarse-grained-level, downstream signaling/regulatory molecules that can diffuse at a larger length-scale.

CONCLUSION

The main goal of this work is to elucidate the spatially extended dynamics of common network motifs implicated in cellular decision-making: toggle switch, toggle triad, and repressilator. We highlight the different patterns observed for varying durations under diverse parameter regimes, thus offering better understanding of design principles of spatial patterns, and pinpointing specific network topologies underlying reaction−diffusion systems. These results pave the way for further multiscale spatiotemporal investigations of cellular-decision-making-regulatory-networks and for deciphering tissue-level patterning in various physiological and diseased scenarios.

METHODS AND MATERIALS

Analytical Formalism. We have studied few two- and three-gene regulatory network motifs that exhibit inherent multistable and oscillatory behaviors, viz., genetic toggle switch, genetic toggle switch coupled with double self-activation, toggle triad, and repressilator. We have written down the sets of partial differential equations representing the reaction−diffusion systems for each of these motifs. Numerically solving the reaction systems (without including the term for the diffusing molecules), we first find the sets of real solutions (coordinates) for the stable fixed points/saddle nodes of the multistable/oscillatory states of the motifs. Linearizing around the stable fixed points/saddle modes, we obtain the linear stability matrix $\mathcal{S}$. Solving the matrix $\mathcal{S}$, we find the traces, determinants, and eigenvalues for the systems, the signs and types of which represent the stability of the systems (refer to text of the Supporting Information for the detailed analytical treatment for each motif). We follow the same analytical treatment with molecular diffusion in one- and two-dimensional space. The resultant trace, determinant and eigenvalues of the reaction−diffusion systems (diffusive GRNs) are functions of the wavenumber k (see text in the Supporting Information for details). To make the distinctions clear and comprehensible, the detailed analytical treatment for the reaction systems and reaction−diffusion systems have been done (see the Supporting Information, text), separately for all the GRNs.

Simulation Details. *Temporal Dynamics of the GRNs.* To solve the coupled ordinary differential equations (ODEs) (equations written in Supporting Information) of the network motif interactions, we integrate the ODEs using the MATLAB (MathWorks Inc.) ode45 solver. We solve the ODEs for 100 initial conditions chosen from the range $[0, 1.5 \times g_A/\gamma_A]$ for total time of 200 units.

Bifurcation Diagram. To calculate and plot the bifurcation diagrams of the coupled ODEs, we used MATCONT[76] (a bifurcation analysis tool in MATLAB (MathWorks Inc.)).

Phase Diagram. We first divided the phase space in 50×50 cells. Then, for each cell, we calculated 50 trajectories, each starting with different initial conditions. We then calculate the number of states from these trajectories and plot the heatmap of the phase space.

Spatiotemporal Dynamics in One Dimension. Consider a one-dimensional chain of cells, each having a toggle switch with diffusing molecules. To solve the reaction diffusion system in 1 dimension we used the pdepe solver in MATLAB. We solve the system for 1D array of 400 cells with the Neumann boundary condition.

Spatiotemporal Dynamics in Two Dimensions. Now, we consider a two-dimensional square lattice of population of cells, each having a toggle switch with diffusing molecules. To solve this system, we wrote a solver using central difference in space and forward difference in time (in python). We divided the space into lattice with 100×100 points and used Neumann boundary conditions. The initial levels of the proteins is chosen from the range $[0, 1.5 \times g_A/\gamma_A]$.

ASSOCIATED CONTENT

Data Availability Statement

All codes are publicly available on the GitHub page of D.S. (https://github.com/Divyoj-Singh/Spatial_patterning_GRNs).

Supporting Information

The Supporting Information is available free of charge at https://pubs.acs.org/doi/10.1021/acsomega.2c04581.

Detailed analytical formulation (governing ODEs and PDEs, stability matrix, trace, determinant, eigenvalues, and conditions for diffusive instability) of reaction and reaction−diffusion systems in one- and two-dimensional space, case studies and mathematical calculation for fundamental multistable and oscillatory gene regulatory network motifs— toggle switch, toggle switch with double self-activation, toggle triad and repressilator (as a limiting case of toggle triad), and supporting video captions (PDF)

Supporting video files (ZIP)

AUTHOR INFORMATION

Corresponding Authors

Ushasi Roy − *Centre for BioSystems Science and Engineering, Indian Institute of Science, Bangalore 560012, India;* orcid.org/0000-0003-3059-6661; Email: ushasiroy@iisc.ac.in

Mohit Kumar Jolly − *Centre for BioSystems Science and Engineering, Indian Institute of Science, Bangalore 560012, India*; Email: mkjolly@iisc.ac.in

Authors

Divyoj Singh − *Undergraduate Programme, Indian Institute of Science, Bangalore 560012, India*

https://doi.org/10.1021/acsomega.2c04581
ACS Omega 2023, 8, 3713−3725

Navin Vincent − *Undergraduate Programme, Indian Institute of Science, Bangalore 560012, India;* orcid.org/0000-0003-2894-6319

Chinmay K. Haritas − *Undergraduate Programme, Indian Institute of Science, Bangalore 560012, India*

Complete contact information is available at: https://pubs.acs.org/10.1021/acsomega.2c04581

Author Contributions

¶Co-first authors Ushasi Roy and Divyoj Singh.

Author Contributions

§Co-second authors Navin Vincent and Chinmay K. Haritas.

Author Contributions

U.R. and M.K.J. planned and led the work. U.R., D.S., N.V., and C.K.H. carried out the research. U.R. and D.S. prepared the initial manuscript. U.R., D.S., and M.K.J. finalized the draft and made intellectual contributions. U.R. and D.S. contributed equally to the work, are co-first authors, and can exchange the author order in their CV. N.V. and C.K.H. contributed equally to the work, are co-second authors, and can exchange the author-order in their CV.

Notes

The authors declare no competing financial interest.

■ ACKNOWLEDGMENTS

U.R. acknowledges a C. V. Raman Postdoctoral Fellowship from the Indian Institute of Science, Bangalore, India. D.S., N.V., and C.K.H. are supported by KVPY fellowships awarded by Department of Science and Technology (DST), Government of India. M.K.J. is supported by a Ramanujan Fellowship (SB/S2/RJN 049/2018) awarded by the Science and Engineering Research Board (SERB), DST, Government of India, and by the Infosys Foundation, Bangalore, India.

■ REFERENCES

(1) DiNardo, S.; Heemskerk, J.; Dougan, S.; O'Farrell, P. H. The making of a maggot: patterning the Drosophila embryonic epidermis. *Current Opinion in Genetics & Development* **1994**, *4*, 529−534.

(2) Lopes, F. J.; Vieira, F. M.; Holloway, D. M.; Bisch, P. M.; Spirov, A. V. Spatial bistability generates hunchback expression sharpness in the Drosophila embryo. *PLoS Computational Biology* **2008**, *4*, No. e1000184.

(3) Herrera-Delgado, E.; Perez-Carrasco, R.; Briscoe, J.; Sollich, P. Memory functions reveal structural properties of gene regulatory networks. *PLoS Computational Biology* **2018**, *14*, No. e1006003.

(4) Ermentrout, B. Neural networks as spatio-temporal pattern-forming systems. *Rep. Prog. Phys.* **1998**, *61*, 353.

(5) Futahashi, R.; Shirataki, H.; Narita, T.; Mita, K.; Fujiwara, H. Comprehensive microarray-based analysis for stage-specific larval camouflage pattern-associated genes in the swallowtail butterfly, Papilio xuthus. *BMC Biology* **2012**, *10*, 1−21.

(6) Meinhardt, H. A model for pattern formation of hypostome, tentacles, and foot in hydra: how to form structures close to each other, how to form them at a distance. *Dev. Biol.* **1993**, *157*, 321−333.

(7) Briscoe, J.; Small, S. Morphogen rules: design principles of gradient-mediated embryo patterning. *Development* **2015**, *142*, 3996−4009.

(8) Lawrence, P. A.; Struhl, G. Morphogens, Compartments, and Pattern: Lessons from Drosophila? *Cell* **1996**, *85*, 951−961.

(9) Perkins, M. L. Implications of diffusion and time-varying morphogen gradients for the dynamic positioning and precision of bistable gene expression boundaries. *PLOS Computational Biology* **2021**, *17*, No. e1008589.

(10) Turing, A. M. The chemical basis of morphogenesis. *Bulletin of Mathematical Biology* **1990**, *52*, 153−197.

(11) Zaikin, A.; Zhabotinsky, A. Concentration wave propagation in two-dimensional liquid-phase self-oscillating system. *Nature* **1970**, *225*, 535−537.

(12) Winfree, A. T. Spiral waves of chemical activity. *Science* **1972**, *175*, 634−636.

(13) Gierer, A.; Meinhardt, H. A theory of biological pattern formation. *Kybernetik* **1972**, *12*, 30−39.

(14) Castets, V.; Dulos, E.; Boissonade, J.; De Kepper, P. Experimental evidence of a sustained standing Turing-type nonequilibrium chemical pattern. *Phys. Rev. Lett.* **1990**, *64*, 2953.

(15) De Kepper, P.; Castets, V.; Dulos, E.; Boissonade, J. Turing-type chemical patterns in the chlorite-iodide-malonic acid reaction. *Physica D: Nonlinear Phenomena* **1991**, *49*, 161−169.

(16) Sanz-Anchelergues, A.; Zhabotinsky, A. M.; Epstein, I. R.; Munuzuri, A. P. Turing pattern formation induced by spatially correlated noise. *Phys. Rev. E* **2001**, *63*, 056124.

(17) Othmer, H. G.; Scriven, L. Instability and dynamic pattern in cellular networks. *J. Theor. Biol.* **1971**, *32*, 507−537.

(18) Lengyel, I.; Epstein, I. R. A chemical approach to designing Turing patterns in reaction−diffusion systems. *Proc. Natl. Acad. Sci. U. S. A.* **1992**, *89*, 3977−3979.

(19) Cross, M. C.; Hohenberg, P. C. Pattern formation outside of equilibrium. *Rev. Mod. Phys.* **1993**, *65*, 851.

(20) Hsia, J.; Holtz, W. J.; Huang, D. C.; Arcak, M.; Maharbiz, M. M. A feedback quenched oscillator produces turing patterning with one diffuser. *PLoS Computational Biology* **2012**, *8*, No. e1002331.

(21) Miyazako, H.; Hori, Y.; Hara, S.Turing instability in reaction−diffusion systems with a single diffuser: characterization based on root locus. *52nd IEEE Conference on Decision and Control*; 2013; pp 2671−2676.

(22) Payne, S.; Li, B.; Cao, Y.; Schaeffer, D.; Ryser, M. D.; You, L. Temporal control of self-organized pattern formation without morphogen gradients in bacteria. *Molecular Systems Biology* **2013**, *9*, 697.

(23) Cao, Y.; Ryser, M. D.; Payne, S.; Li, B.; Rao, C. V.; You, L. Collective space-sensing coordinates pattern scaling in engineered bacteria. *Cell* **2016**, *165*, 620−630.

(24) Cohen, D. J.; Morfino, R. C.; Maharbiz, M. M. A modified consumer inkjet for spatiotemporal control of gene expression. *PloS ONE* **2009**, *4*, No. e7086.

(25) Sohka, T.; Heins, R. A.; Ostermeier, M. Morphogen-defined patterning of Escherichia coli enabled by an externally tunable band-pass filter. *Journal of Biological Engineering* **2009**, *3*, 1−9.

(26) Basu, S.; Mehreja, R.; Thiberge, S.; Chen, M.-T.; Weiss, R. Spatiotemporal control of gene expression with pulse-generating networks. *Proc. Natl. Acad. Sci. U. S. A.* **2004**, *101*, 6355−6360.

(27) Basu, S.; Gerchman, Y.; Collins, C. H.; Arnold, F. H.; Weiss, R. A synthetic multicellular system for programmed pattern formation. *Nature* **2005**, *434*, 1130−1134.

(28) Luo, N.; Wang, S.; You, L. Synthetic pattern formation. *Biochemistry* **2019**, *58*, 1478−1483.

(29) van Zon, J. S.; Morelli, M. J.; Tănase-Nicola, S.; ten Wolde, P. R. Diffusion of transcription factors can drastically enhance the noise in gene expression. *Biophys. J.* **2006**, *91*, 4350−4367.

(30) Tkačik, G.; Bialek, W. Diffusion, dimensionality, and noise in transcriptional regulation. *Phys. Rev. E* **2009**, *79*, 051901.

(31) Cottrell, D.; Swain, P. S.; Tupper, P. F. Stochastic branching-diffusion models for gene expression. *Proc. Natl. Acad. Sci. U. S. A.* **2012**, *109*, 9699−9704.

(32) Barbier, I.; Perez-Carrasco, R.; Schaerli, Y. Controlling spatiotemporal pattern formation in a concentration gradient with a synthetic toggle switch. *Molecular Systems Biology* **2020**, *16*, No. e9361.

(33) Perez-Carrasco, R.; Barnes, C. P.; Schaerli, Y.; Isalan, M.; Briscoe, J.; Page, K. M. Combining a toggle switch and a repressilator within the AC-DC circuit generates distinct dynamical behaviors. *Cell Systems* **2018**, *6*, 521−530.

(34) Diambra, L.; Senthivel, V. R.; Menendez, D. B.; Isalan, M. Cooperativity to increase Turing pattern space for synthetic biology. *ACS Synth. Biol.* **2015**, *4*, 177−186.
(35) Gardner, T. S.; Cantor, C. R.; Collins, J. J. Construction of a genetic toggle switch in Escherichia coli. *Nature* **2000**, *403*, 339−342.
(36) Jia, D.; Jolly, M. K.; Harrison, W.; Boareto, M.; Ben-Jacob, E.; Levine, H. Operating principles of tristable circuits regulating cellular differentiation. *Physical Biology* **2017**, *14*, 035007.
(37) Duddu, A. S.; Sahoo, S.; Hati, S.; Jhunjhunwala, S.; Jolly, M. K. Multi-stability in cellular differentiation enabled by a network of three mutually repressing master regulators. *J. R. Soc., Interface* **2020**, *17*, 20200631.
(38) Elowitz, M. B.; Leibler, S. A synthetic oscillatory network of transcriptional regulators. *Nature* **2000**, *403*, 335−338.
(39) Zhou, J. X.; Huang, S. Understanding gene circuits at cell-fate branch points for rational cell reprogramming. *Trends in Genetics* **2011**, *27*, 55−62.
(40) Lopes, F. J.; Spirov, A. V.; Bisch, P. M. The role of Bicoid cooperative binding in the patterning of sharp borders in Drosophila melanogaster. *Dev. Biol.* **2012**, *370*, 165−172.
(41) Igoshin, O. A.; Alves, R.; Savageau, M. A. Hysteretic and graded responses in bacterial two-component signal transduction. *Mol. Microbiol.* **2008**, *68*, 1196−1215.
(42) Venturelli, O. S.; El-Samad, H.; Murray, R. M. Synergistic dual positive feedback loops established by molecular sequestration generate robust bimodal response. *Proc. Natl. Acad. Sci. U. S. A.* **2012**, *109*, E3324−E3333.
(43) Venturelli, O. S.; Zuleta, I.; Murray, R. M.; El-Samad, H. Population diversification in a yeast metabolic program promotes anticipation of environmental shifts. *PLoS Biology* **2015**, *13*, No. e1002042.
(44) Lu, M.; Jolly, M. K.; Levine, H.; Onuchic, J. N.; Ben-Jacob, E. MicroRNA-based regulation of epithelial-hybrid-mesenchymal fate determination. *Proc. Natl. Acad. Sci. U.S.A.* **2013**, *110*, 18144−18149.
(45) Hari, K.; Sabuwala, B.; Subramani, B. V.; La Porta, C. A.; Zapperi, S.; Font-Clos, F.; Jolly, M. K. Identifying inhibitors of epithelial-mesenchymal plasticity using a network topology-based approach. *NPJ. Systems Biology and Applications* **2020**, *6*, 1−12.
(46) Lu, M.; Jolly, M. K.; Gomoto, R.; Huang, B.; Onuchic, J.; Ben-Jacob, E. Tristability in cancer-associated microRNA-TF chimera toggle switch. *J. Phys. Chem. B* **2013**, *117*, 13164−13174.
(47) Huang, S.; Guo, Y.-P.; May, G.; Enver, T. Bifurcation dynamics in lineage-commitment in bipotent progenitor cells. *Dev. Biol.* **2007**, *305*, 695−713.
(48) Jolly, M. K.; Boareto, M.; Huang, B.; Jia, D.; Lu, M.; Ben-Jacob, E.; Onuchic, J. N.; Levine, H. Implications of the hybrid epithelial/mesenchymal phenotype in metastasis. *Frontiers in Oncology* **2015**, *5*, 155.
(49) Jolly, M. K.; Tripathi, S. C.; Jia, D.; Mooney, S. M.; Celiktas, M.; Hanash, S. M.; Mani, S. A.; Pienta, K. J.; Ben-Jacob, E.; Levine, H. Stability of the hybrid epithelial/mesenchymal phenotype. *Oncotarget* **2016**, *7*, 27067.
(50) Jia, D.; Jolly, M. K.; Tripathi, S. C.; Den Hollander, P.; Huang, B.; Lu, M.; Celiktas, M.; Ramirez-Peña, E.; Ben-Jacob, E.; Onuchic, J. N.; et al. Distinguishing mechanisms underlying EMT tristability. *Cancer Convergence* **2017**, *1*, 1−19.
(51) Huang, S. Hybrid T-helper cells: stabilizing the moderate center in a polarized system. *PLoS Biology* **2013**, *11*, No. e1001632.
(52) Tripathi, S.; Kessler, D. A.; Levine, H. Biological Networks Regulating Cell Fate Choice Are Minimally Frustrated. *Phys. Rev. Lett.* **2020**, *125*, 1−6.
(53) Novák, B.; Tyson, J. J. Design principles of biochemical oscillators. *Nat. Rev. Mol. Cell Biol.* **2008**, *9*, 981−991.
(54) Raj, A.; Van Oudenaarden, A. Nature, nurture, or chance: stochastic gene expression and its consequences. *Cell* **2008**, *135*, 216−226.
(55) Riaz, S. S.; Ray, D. S. Diffusion and mobility driven instabilities in a reaction−diffusion system: a review. *Ind. J. Phys.* **2007**, *81*, 1177−1204.
(56) Guin, L. N.; Haque, M.; Mandal, P. K. The spatial patterns through diffusion-driven instability in a predator−prey model. *Applied Mathematical Modelling* **2012**, *36*, 1825−1841.
(57) Li, Y.; Liu, H.; Wei, Y.; Ma, M. Turing pattern of a reaction−diffusion predator-prey model with weak Allee effect and delay. *Journal of Physics: Conference Series* **2020**, *1707*, 012025.
(58) Li, Y. X.; Liu, H.; Wei, Y. M.; Ma, M.; Ma, G.; Ma, J. Y. Population Dynamic Study of Prey-Predator Interactions with Weak Allee Effect, Fear Effect, and Delay. *Journal of Mathematics* **2022**, *2022*, 1−15.
(59) van Gestel, J.; Bareia, T.; Tenennbaum, B.; Dal Co, A.; Guler, P.; Aframian, N.; Puyesky, S.; Grinberg, I.; D'Souza, G. G.; Erez, Z.; Ackermann, M.; Eldar, A. Short-range quorum sensing controls horizontal gene transfer at micron scale in bacterial communities. *Nat. Commun.* **2021**, *12*, 1−11.
(60) Duran-Nebreda, S.; Pla, J.; Vidiella, B.; Piñero, J.; Conde-Pueyo, N.; Solé, R. Synthetic Lateral Inhibition in Periodic Pattern Forming Microbial Colonies. *ACS Synth. Biol.* **2021**, *10*, 277−285.
(61) Oelker, A.; Horger, T.; Kuttler, C. From Staphylococcus aureus gene regulation to its pattern formation. *Journal of Mathematical Biology* **2019**, *78*, 2207−2234.
(62) Gomez, M. M.; Arcak, M. A tug-of-war mechanism for pattern formation in a genetic network. *ACS Synth. Biol.* **2017**, *6*, 2056−2066.
(63) Dal Co; van Vliet, S.; Kiviet, D. J.; Schlegel, S.; Ackermann, M. Short-range interactions govern the dynamics and functions of microbial communities. *Nature Ecology & Evolution* **2020**, *4*, 366−375.
(64) Kondo, S. The reaction−diffusion system: a mechanism for autonomous pattern formation in the animal skin. *Genes to Cells* **2002**, *7*, 535−541.
(65) Murray, J. D. A pre-pattern formation mechanism for animal coat markings. *J. Theor. Biol.* **1981**, *88*, 161−199.
(66) Chuong, C.-M.; Richardson, M. K. Pattern formation today. *International Journal of Developmental Biology* **2009**, *53*, 653.
(67) Meinhardt, H.*Models of biological pattern formation*; Academic: New York, 1982; p 118.
(68) Meinhardt, H.*The algorithmic beauty of sea shells*; Springer Science & Business Media: 2009.
(69) Bode, P. M.; Bode, H. R. Formation of pattern in regenerating tissue pieces of Hydra attenuata: II. Degree of proportion regulation is less in the hypostome and tentacle zone than in the tentacles and basal disc. *Dev. Biol.* **1984**, *103*, 304−312.
(70) Yates, K.; Pate, E. A cascading development model for amphibian embryos. *Bulletin of Mathematical Biology* **1989**, *51*, 549−578.
(71) Schiffmann, Y. An hypothesis: phosphorylation fields as the source of positional information and cell differentiation—(cAMP, ATP) as the universal morphogenetic Turing couple. *Prog. Biophys. Mol. Biol.* **1991**, *56*, 79−105.
(72) Fritsch, C.; Ploeger, G.; Arndt-Jovin, D. J. Drosophila under the lens: imaging from chromosomes to whole embryos. *Chromosome Research* **2006**, *14*, 451−464.
(73) Barbier, I.; Kusumawardhani, H.; Schaerli, Y. Engineering synthetic spatial patterns in microbial populations and communities. *Curr. Opin. Microbiol.* **2022**, *67*, 102149.
(74) Tompkins, N.; Li, N.; Girabawe, C.; Heymann, M.; Ermentrout, G. B.; Epstein, I. R.; Fraden, S. Testing Turing's theory of morphogenesis in chemical cells. *Proc. Natl. Acad. Sci. U. S. A.* **2014**, *111*, 4397−4402.
(75) Sarkar, S. Concentration dependence of diffusion-limited reaction rates and its consequences. *Physical Review X* **2020**, *10*, 041032.
(76) Dhooge, A.; Govaerts, W.; Kuznetsov, Y. A.; Meijer, H. G. E.; Sautois, B. New features of the software MatCont for bifurcation analysis of dynamical systems. *Mathematical and Computer Modelling of Dynamical Systems* **2008**, *14*, 147−175.

https://doi.org/10.1021/acsomega.2c04581
ACS Omega 2023, 8, 3713−3725